Pulse-shape control of two-color interference in high-order-harmonic generation

K. R. Hamilton, H. W. van der Hart, and A. C. Brown

Centre for Theoretical Atomic, Molecular and Optical Physics, Queen's University Belfast, Belfast BT7 1NN, United Kingdom of Great Britain and Northern Ireland

We report on calculations of harmonic generation by neon in a mixed (800-nm + time-delayed 400-nm) laser pulse scheme. In contrast with previous studies we employ a short (few-cycle) 400-nm pulse, finding that this affords control of the interference between electron trajectories contributing to the cutoff harmonics. The inclusion of the 400-nm pulse enhances the yield and cutoff energy, both of which exhibit a strong dependence on the time delay between the two pulses. Using a combination of time-dependent R-matrix theory and a classical trajectory model, we assess the mechanisms leading to these effects.

I. INTRODUCTION

The process of high-order-harmonic generation (HHG) has been the driving force behind countless new developments in ultrafast laser technologies over the past decade. HHG has been used to create both short-duration [1] and high-energy [2] laser pulses and can also be used directly in atomic [3] and molecular spectroscopy [4] to elucidate the attosecond-scale dynamics of electrons.

HHG is commonly described by the classical three-step model in which an electron (i) tunnels through the laser-suppressed Coulomb barrier, (ii) is accelerated by the field, and (iii) recombines with its parent atom emitting a high-energy photon, all within a single cycle of the driving laser field [5]. Analysis of the electron motion reveals two classes of trajectory. The so-called long and short trajectories represent two distinct pathways leading to the same recollision energy. Importantly, the cutoff (highest) energy trajectories arise when the long and short trajectories coalesce. It has been shown that interference between these pathways leads to an Airy pattern in the harmonic plateau [6].

The study of spectral caustics in HHG is an extension of this interference effect. Caustics arise in the analysis of ray optics: where multiple rays coalesce a sharp peak, or caustic, appears in the emitted radiation. This enhancement is predicted by catastrophe theory, and is due to a singularity in the spectral density. In HHG, caustics result from the coalescence of more than two electron trajectories in the same spectral region, which can be engineered by adding a second color to the driving laser pulse. The second color breaks the symmetry of the process, splitting the electron trajectories into two further classes. The so-called upper and lower branch trajectories (named as they yield higher or lower cutoff energies than the equivalent one-color trajectories) can then interfere and, when they coalesce at the cutoff energy, yield a dramatic enhancement in the harmonic spectrum [7,8].

Such interference between trajectories represents an attractive means of probing the quantum nature of the HHG process, which has been understood primarily as a strong-field (classical) process. However, this is experimentally challenging, because the measured harmonic spectrum arises from the coherent response of many atoms and, depending on the experimental conditions, only either the short or long trajectories can be appropriately phase matched. Additionally, in

a two-color field, the upper branch trajectories have a reduced ionization and recollision probability relative to the lower branch. Recently, however, it was shown that a shape resonance in the harmonic spectrum can compensate for these factors, and reveal the spectral interference of the relevant trajectories [8].

The manipulation of electron trajectories with two color fields has been realized in various schemes. Schafer and coworkers proposed the use of a combined infrared (IR)/extreme ultraviolet (XUV) scheme to control the electron trajectories [9]. More recently the XUV-initiated HHG scheme has been applied to monitor core-hole dynamics in small molecules [10], and to elucidate the contribution of both inner and outer valence electrons to the HHG spectrum [11].

A more established technique involves the use of two colors in the visible-IR range, and in particular using a driving pulse and its second harmonic ($\omega + 2\omega$) has been well studied. The inclusion of the second harmonic has been shown to enhance the high-harmonic yield [12] and extend the cutoff energy of the harmonic spectrum [13]. Thus, two-color fields have been used extensively for the generation of supercontinua in the XUV range [14,15], the spectral shaping of attosecond pulse trains [16], and quantum path selection in HHG [17].

In all previous studies, the second harmonic is included as a long-duration dressing field which imparts some phase-dependent effect to the harmonic spectrum. In the present paper we will instead consider the interference between electron trajectories driven by two few-cycle pulses.

We obtain the harmonic spectra using the *ab initio* time-dependent R-matrix method known as RMT [18]. RMT has been used to investigate various strong-field phenomena, including multielectron correlation in doubly and core-excited states in Ne [19], electron recollision in F^- [20], IR-assisted photoionization of Ne^+ [21], and HHG from noble gas atoms in the NIR regime [11,22]. A predecessor to the RMT method was also used extensively to study harmonic generation in a variety of targets in the UV-visible range [23–26]. The RMT approach has two defining capabilities. First, the code is optimized to run on massively parallel (>1000 cores) machines, thus making the extension to challenging physical systems tractable. Second, the RMT approach can be applied to general multielectron systems—including open-shell atoms and ions—with a full description of electron correlation effects.

Here we use the *ab initio* RMT method to apply a quantitative analysis to spectral caustics in two-color HHG

schemes. We first give an overview of the RMT method and the calculation parameters employed, then present results of calculations of the harmonic spectrum for a neon atom in a combined 800/400-nm pulse scheme.

II. TIME-DEPENDENT *R*-MATRIX THEORY

The R matrix with time-dependence method (RMT) employs the well-known R-matrix paradigm of dividing configuration space into two separate regions, in this case over the radial coordinate of an ejected electron. In an inner region (close to the nucleus) all electron-electron interactions are taken into account while in the outer region an ejected electron is sufficiently far from the residual ion that the effect of electron exchange can be neglected. The most appropriate numerical method for solving the time-dependent Schrödinger equation (TDSE) is employed in each region and, at variance with other R-matrix-based approaches, the wave function itself is matched explicitly at the boundary rather than via an R matrix [18].

In the inner region the time-dependent N-electron wave function is represented over an R-matrix basis with time-dependent coefficients. The basis is constructed from the $N - 1$ electron-states of the residual ion coupled to a complete set of single-electron functions representing the ejected electron. Additional N-electron correlation functions can be added to the basis set to improve the accuracy of the wave function. In the outer region, the wave function is described in terms of residual-ion states coupled with the radial wave function of the ejected electron and is expressed explicitly on a finite-difference grid. The two region wave functions are then matched directly at the boundary in two directions. The outer region finite-difference grid is extended into the inner region and the inner region wave function is evaluated on this grid. This provides the boundary condition for the solution of the TDSE in the outer region. A derivative of the outer region wave function at the boundary is also made available to the inner region, enabling the inner region wave function to be updated. The wave function is propagated in the length gauge, as it has been found to give better results with the atomic structure description employed in time-dependent R-matrix calculations [27].

The harmonic spectra are obtained by evaluating the time-dependent expectation value of the dipole velocity, then Fourier transforming and squaring it, thus,

$$\dot{\mathbf{d}}(t) = \frac{d}{dt} \langle \Psi(t) | -e\mathbf{z} | \Psi(t) \rangle, \tag{1}$$

where $\mathbf{z}$ is the total position operator along the laser polarization axis and Ψ is the wave function. It is also possible to calculate the spectra using the expectation value of the dipole length [28], and within our simulations this is used as a check for accuracy. Indeed the spectra produced from each method show excellent agreement with each other until well past the cutoff energy. The spectra shown in the present paper are those calculated from the dipole velocity.

To aid our analysis of the harmonic spectra we perform classical trajectory simulations based on the three-step model [5]. We assume an electron is tunnel ionized into the continuum with zero initial velocity, and, for each possible ionization time, we determine the electron's velocity and position by integrating over the acceleration in the two-color field. We note that this model does not account for any effect of the atomic potential. Trajectories which return again to the origin represent recolliding electrons which give rise to harmonic generation. The energy of this emitted harmonic light can then be calculated from the electron's recollision energy and the ionization potential.

III. CALCULATION PARAMETERS

The neon atom is described within an R-matrix inner region with a radius of 20 a.u. and an outer region of 2500 a.u. An absorbing boundary, beginning at 1500 a.u., is included to prevent reflections of the wave function. The finite-difference grid spacing in the outer region is 0.08 a.u. and the time step for the wave-function propagation is 0.01 a.u. The description of neon includes all available $2s^2 2p^5 \epsilon \ell$ and $2s 2p^6 \epsilon \ell$ channels up to a maximum total angular momentum of $L_{\max} = 79$. The inner region continuum functions are constructed using a set of 50 B splines of order 9 for each available angular momentum of the outgoing electron.

We employ a mixed laser pulse scheme comprising a fundamental (800-nm) pulse and its second harmonic (400 nm). In every mixed laser pulse scheme employed the pulses are linearly polarized and parallel. The intensities of the 800- and 400-nm pulses are fixed at 4×10^{14} W/cm^2 (corresponding to a ponderomotive energy of 24 eV) and 4×10^{13} W/cm^2, respectively. Both pulses employ a sin^2 ramp on/off and are, unless otherwise stated, six cycles in duration (three cycles ramp on, three cycles ramp off). The time delay is measured between the central peaks of the two pulses, and a negative time delay corresponds to the 400-nm pulse arriving first. We increment the time delay in steps of 0.1 fs.

IV. RESULTS

Figure 1(a) shows the harmonic spectra obtained from neon irradiated by a six-cycle 800-nm (ω) pulse and a time-delayed six-cycle 400-nm (2ω) pulse. The inclusion of the 2ω pulse breaks the symmetry of the three step process, and stimulates the generation of even harmonics [29]. The two-color field also elicits an enhancement of up to four orders of magnitude in the harmonic emission compared to the primary field alone (not shown), particularly in the cutoff region [12]. This is one to two orders of magnitude higher than the enhancement achieved by simply increasing the intensity of the primary field by 10% to match the combined peak intensity of the two-color field.

This enhancement is manifest most clearly in the appearance of the distinctive swallowtail caustics in the cutoff harmonics. These sharp peaks in harmonic emission represent a singularity in the harmonic emission, caused by the coalescence of multiple electron trajectories in the two-color field [7]. Changing the time delay between the ω and 2ω pulses changes the phase relationship between the interfering trajectories, shifting the coalescence to higher energy and leading to the two "arms" of the swallowtail. The series of swallowtails which peak at the cutoff energy and decrease in intensity with decreasing harmonic photon energy describe an Airy pattern [6].
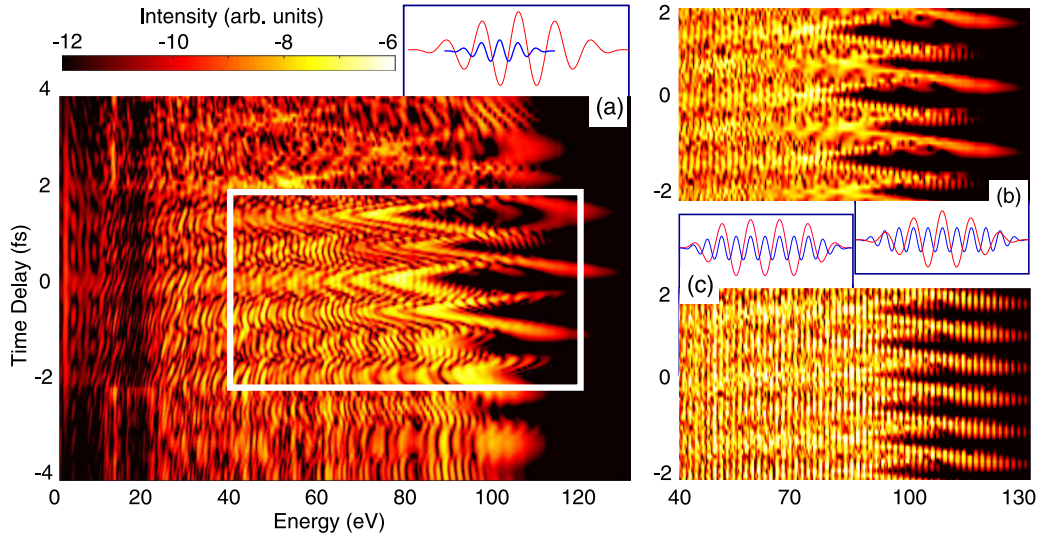
FIG. 1. Harmonic spectra produced by neon irradiated by (a) a six-cycle, 800-nm pulse and time-delayed six-cycle, 400-nm pulse; (b) a six-cycle, 800-nm pulse and a time-delayed 12-cycle, 400-nm pulse; and (c) a six-cycle, 800-nm pulse with two cycles at peak intensity and a time-delayed 12-cycle, 400-nm pulse. Insets show pictorially the two laser fields used.

The swallowtail caustics are most clearly visible when two short pulses are used [Fig. 1(a)], but the overall yield is increased by the use of a longer 2ω pulse. Figures 1(b) and 1(c) show the spectra produced using a 12-cycle 400-nm pulse. In both cases the 400-nm pulse has a three-cycle $\sin^2$ ramp on and off, with six cycles at peak intensity (3-6-3); in Fig. 1(b) the 800-nm pulse has a 3-3 form while in Fig. 1(c) it has a 2-2-2 form. Using a long 2ω pulse is more similar in spirit to previous studies in this field, where the second harmonic can be treated as a dressing field which imparts a phase dependent enhancement or suppression on the harmonic yield [12–17].

Using a long 2ω pulse yields an increase in harmonic emission relative to the short-2ω-pulse spectra in Fig. 1(a). The 2ω field is present for the duration of the 800-nm pulse, and thus affects electron trajectories originating earlier or later in the fundamental pulse. Thus the emission is also less concentrated in the cutoff region such that the entire plateau is enhanced. Furthermore, the interference patterns in the time-delay spectra are strongly modified by the shape of the pulses. Changing from a 3-3 to a 2-2-2 pulse shape is similar to broadening the carrier envelope of a Gaussian 800-nm field: with this profile there is no longer a single central peak. Thus each harmonic energy is sourced by trajectories on multiple cycles, and the interference between them appears as the comblike fringes in Fig. 1(c). The arms of the swallowtail caustic are still visible in the cutoff region, but the singular enhancement at the point of the caustics is somewhat bleached by the overall increase in the harmonic yield. Changing the pulse profile also has the effect of shifting the caustic to higher energy, as shown in Fig. 2, because the trajectories leading to the caustic are now driven by higher intensity cycles of the 800-nm pulse. For the same reason, the swallowtail caustic which appears for a delay of ≈ -0.5 fs in Figs. 2(a) and 2(b) is at higher energy than the main caustic at $\approx +0.17$ fs: the particular half cycle of the 800-nm pulse which drives the cutoff trajectories is stronger, as depicted in Fig. 3(c) compared with Fig. 3(d).
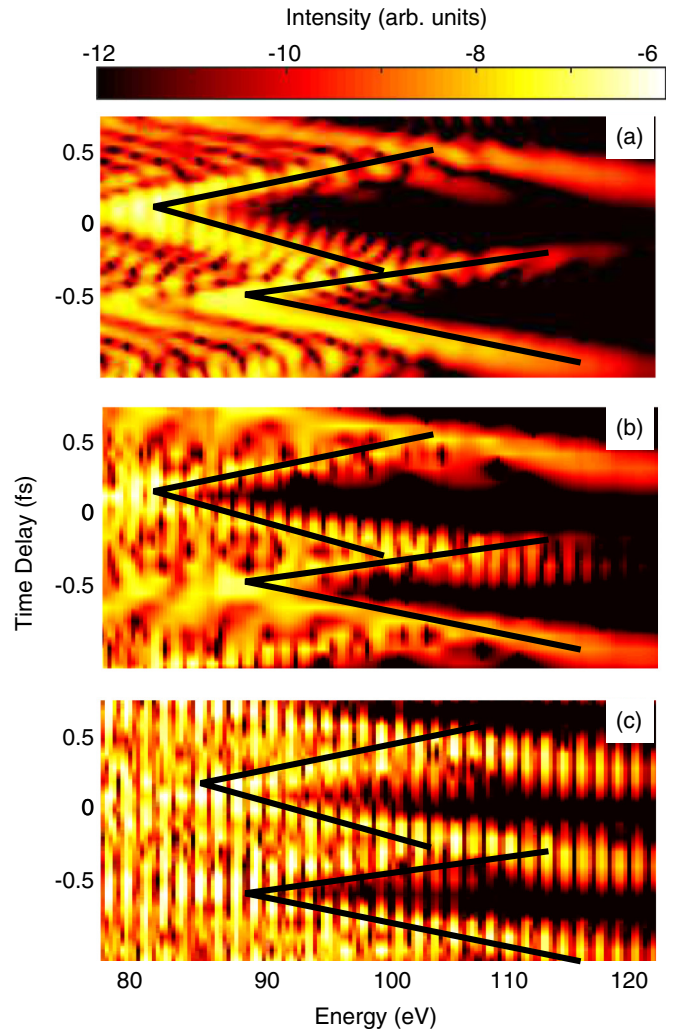

FIG. 2. A zoomed view of the spectral caustics for each of the laser pulse scenarios described in the caption of Fig. 1. The swallowtail caustics are marked with black lines in each.
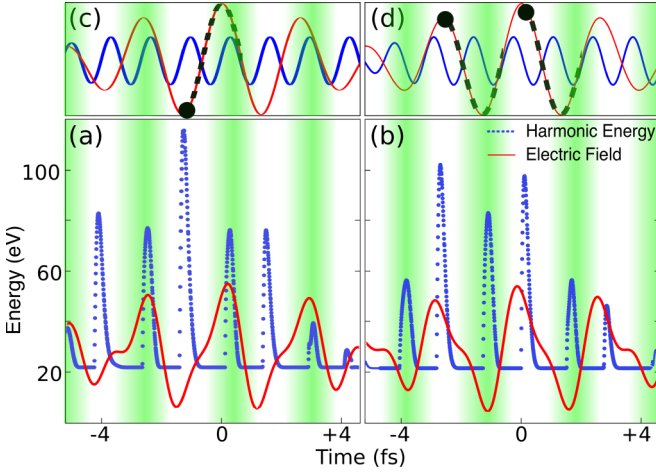
FIG. 3. The harmonic photon energy (blue dots) produced by electrons "born" at a given time during the laser pulse (red line) as calculated by a classical trajectory model, for a time delay of (a) 0.3 fs (2ω peak arriving just after the ω peak) and (b) 1.0 fs (2ω peak arriving just before the ω peak). Panel (a) generates one trajectory with the highest (cutoff) energy, while panel (b) generates two which interfere. The individual 2ω and ω fields are shown in panels (c) and (d) where the positions of the optimal electron emission times are marked by black dots. The green shaded regions correspond to the overlap of two peaks or two troughs, while the unshaded (white) regions correspond to the overlap of a peak and trough. Thus trajectories launched in the green regions do so with higher probability, as the tunnel-ionization probability is increased.

Using a profile with a single central peak yields two different interference structures in the cutoff harmonics in Fig. 1(b)—a long smeared out finger extending to high energy and a lower-energy comblike interference pattern.

We suggest the following interpretation of these interference structures in the strong-field context. The highest-energy trajectories are launched when a (peak) trough of the 2ω field arrives just after a trough (peak) of the ω pulse, i.e., when the vector potentials of the two fields are oppositely oriented (unshaded regions in Fig. 3). In a short pulse, the highest-energy trajectories are launched at the trough one half cycle prior to the central peak [Fig. 3(c): black dot]. Therefore, for delays where a peak of the 400-nm pulse arrives just after the penultimate trough of the 800-nm pulse, there is one trajectory with the highest return energy, which manifests as broad harmonic peaks at the cutoff [22], and appears as the long smeared out fingerlike feature in Fig. 1(b).

By contrast, if troughs of the 400-nm pulse occur just after the penultimate and main peaks of the 800-nm pulse, trajectories of approximately equal return energy are launched from each [Fig. 3(d): black dots]. Interference between harmonic light generated by the two trajectories yields a comblike interference pattern. This picture is supported by classical trajectory calculations, which reveal that the highest-energy harmonics are sourced from one or two cycles of the fundamental pulse depending on the time delay.

Figure 4 shows the cutoff energy and caustic intensity as a function of time delay for the short 2ω pulse scheme used in Fig. 1(a). The caustic intensity is the peak intensity in
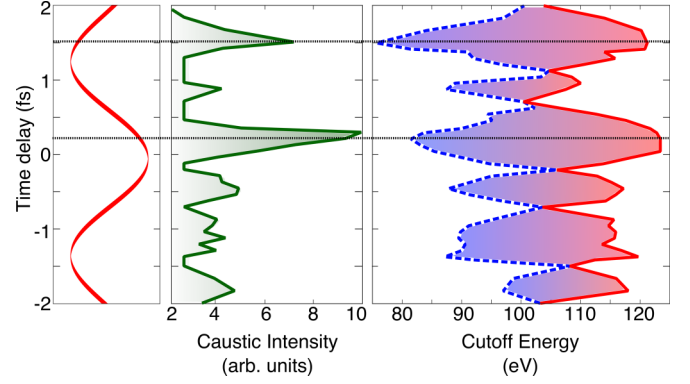

FIG. 4. Intensity of the spectral caustic (central panel) and cutoff energy (right panel) from neon irradiated by short (six-cycle) 800- and 400-nm pulses with varying time delay. The cutoffs of both the first (lower energy: blue dashed line) and second (higher energy: red solid line) plateaus are shown. The 800-nm pulse profile is shown for reference in the left panel. The time delays which give most intense caustic enhancement and the lowest or highest first or second cutoff are marked with the horizontal lines.

the cutoff harmonics and the cutoff energy is extracted for each time delay by sight. We note that there are two cutoff energies as using a two-color field results in HHG spectra with double plateaus [30]. These two plateaus correspond to trajectories launched at a combined peak/peak or peak/trough of the two color field. As a result, the caustic intensity and cutoff energies oscillate with half the period of the 400-nm pulse: The half(800-nm)-cycle symmetry of the three-step HHG mechanism is broken by the inclusion of the 400-nm pulse.

The two cutoff energies are anticorrelated—an extension of the higher-energy cutoff reduces the cutoff energy of the first plateau. At certain time delays the cutoff energies overlap, and we observe a single plateau: for these time delays, classical trajectory calculations reveal that there are trajectories of approximately equal return energy launched on multiple field peaks. The peak caustic intensity occurs when the cutoff of the first plateau is at a minimum. The intensity along the arms of the swallowtail in Fig. 1 then decreases as the pulse arrangement yields higher-energy trajectories at the expense of a lower ionization probability.

Extending the second plateau to higher energy comes at the expense of a reduction of yield in the second plateau. As the cutoff energy increases, the caustic at the first cutoff becomes more intense, dominating the spectrum. The peak caustic intensity occurs when the second cutoff energy is at

TABLE I. The delay time, which gives the peak harmonic emission and highest cutoff energy for neon in an $\omega - 2\omega$ pulse scheme, is an approximately constant phase offset for three different values of the primary (ω) wavelength.

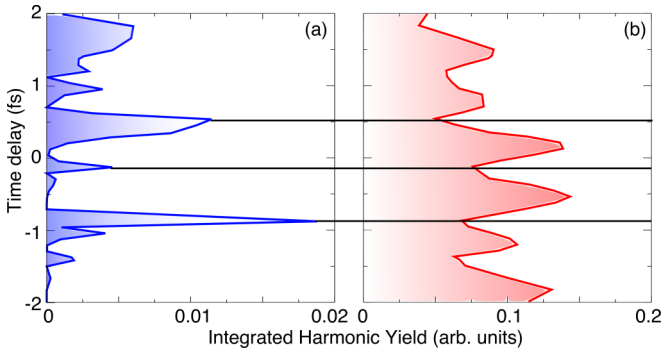| Wavelength (nm)	Period (fs)	Offset (fs)	Phase offset (rad)
600	2.00	0.14	0.44
800	2.67	0.17	0.39
1300	4.33	0.33	0.48

FIG. 5. Integrated harmonic yield of the first (b) and second (a) plateaus arising in the harmonic spectra of neon exposed to two short laser pulses as described in Fig. 1(a). The variation of the yield, as marked by the horizontal lines, is periodic with half the period of the 400-nm pulse.

its highest. This occurs at a time delay of 0.17 fs, not zero delay as might be expected naively. To elucidate this further, we perform calculations for different primary wavelengths, and find that the offset from zero delay is a constant phase difference of approximately $\pi/7$ (Table I).

This offset, approximately 7% of the field period, is the proportion of the pulse peak where the electric field can be considered to be quasistatic (over 97% of its peak strength). Tunnel ionization is most likely in this quasistatic window. For this optimal phase offset the peak of the 2ω pulse arrives just after that of the fundamental pulse, broadening the central peak and enhancing ionization. The green shaded regions of Fig. 3 highlight the trajectories which are launched by such broadened peak. It can be seen that these trajectories yield lower-energy harmonics than those which are launched in the unshaded regions. Thus the most likely ionization event yields the spectral caustic, while at the same time delay much higher-energy trajectories are launched but with vanishingly small probability (Fig. 5). For the two time delays on either side of zero delay which yield the most intense caustics, the yield at the first plateau is three orders of magnitude larger than the yield in the second.

The main caustic (time delay ≈ 0.17 fs) has nearly twice the intensity of the second (time delay ≈ 0.5 fs). This is because the field strength at the central peak is higher than in the penultimate trough. Both of these caustics arise when a peak (trough) of the 2ω pulse arrives just after a peak (trough) of the ω pulse. For a time delay one half cycle of the 2ω pulse sooner or later, the positions of the peaks and troughs of the 400-nm pulse relative to the 800-nm pulse are reversed. A trough of the 2ω pulse occurring after the peak of the 800-nm

pulse results in a shorter, flatter fundamental peak decreasing the ionization probability and therefore the harmonic yield. Thus periodic reduction in cumulative yield, seen as the blue horizontal bands in Fig. 1(a) and more explicitly in Fig. 5, occur when a trough of the 400-nm pulse coincides with the peak of the 800-nm pulse.

V. CONCLUSION

The continued improvement of both large-scale and table-top laser technology has created increased flexibility to shape light pulses, controlling both their spectral and temporal properties [31]. Although an aligned $\omega - 2\omega$ scheme is by no means the most sophisticated or complex arrangement, it nonetheless provides a tractable insight into the strong-field dynamics of atomic electrons. In this paper we have assessed the behavior of a neon atom exposed to such a combination of pulses. While it was previously well known that employing the second harmonic field could substantially increase both the harmonic yield and cutoff, we have seen that using a short, few-cycle 2ω pulse can elicit more interesting behaviors. In particular, a short 2ω pulse can stimulate different interference structures in the harmonic spectrum—leading to spectral caustics and continua or comblike fringes depending on the precise shape of the pulse.

Also, using both the RMT method and a classical trajectory model we are able to assess the mechanisms by which the HHG yield and cutoff are affected. Namely, a broadening of the fundamental peak leads to increased tunnel ionization and thereby increased HHG yield, while a simultaneous narrowing of the previous trough increases the electron excursion time, increasing the recollision velocity and hence the cutoff energy.

With the enhanced ability to shape light pulses in experiment, it will become increasingly important to understand in detail the response of atoms and molecules to more complex arrangements of laser pulses. To this end, it will be interesting to use the capabilities of the RMT method to identify schemes whereby the signatures of multielectron correlation and atomic structure can be extracted from high-order-harmonic spectra.

The data used in this paper may be accessed via Ref. [32].

[1] K. Zhao, Q. Zhang, M. Chini, Y. Wu, X. Wang, and Z. Chang, Tailoring a 67 attosecond pulse through advantageous phase-mismatch, Opt. Lett. **37**, 3891 (2012).

[2] T. Popmintchev *et al.*, Bright Coherent Ultrahigh Harmonics in the keV X-Ray Regime from Mid-Infrared Femtosecond Lasers, Science **336**, 1287 (2012).

[3] T. Morishita, A.-T. Le, Z. Chen, and C. D. Lin, Accurate Retrieval of Structural Information from Laser-Induced Photoelectron and High-Order Harmonic Spectra by Few-Cycle Laser Pulses, Phys. Rev. Lett. **100**, 013903 (2008).

[4] J. Itatani, J. Levesque, D. Zeidler, H. Niikura, H. Pépin, J. C. Kieffer, P. B. Corkum, and D. M. Villeneuve, Tomographic

imaging of molecular orbitals, Nature (London) **432**, 867 (2004).

[5] P. B. Corkum, Plasma Perspective on Strong Field Multiphoton Ionization, Phys. Rev. Lett. **71**, 1994 (1993).

[6] M. V. Frolov, N. L. Manakov, T. S. Sarantseva, and A. F. Starace, Analytic formulae for high harmonic generation, J. Phys. B **42**, 035601 (2009).

[7] O. Raz, O. Pedatzur, B. D. Bruner, and N. Dudovich, Spectral caustics in attosecond science, Nat. Photon. **6**, 170 (2012).

[8] D. Faccialà, S. Pabst, B. D. Bruner, A. G. Ciriolo, S. DeSilvestri, M. Devetta, M. Negro, H. Soifer, S. Stagira, N. Dudovich, and C. Vozzi, Probe of Multielectron Dynamics in Xenon by Caustics in High-Order Harmonic Generation, Phys. Rev. Lett. **117**, 093902 (2016).

[9] K. J. Schafer, M. B. Gaarde, A. Heinrich, J. Biegert, and U. Keller, Strong Field Quantum Path Control Using Attosecond Pulse Trains, Phys. Rev. Lett. **92**, 023003 (2004).

[10] J. Leeuwenburgh, B. Cooper, V. Averbukh, J. P. Marangos, and M. Ivanov, High-Order Harmonic Generation Spectroscopy of Correlation-Driven Electron Hole Dynamics, Phys. Rev. Lett. **111**, 123002 (2013).

[11] A. C. Brown and H. W. van der Hart, Extreme-Ultraviolet-Initated High-Order Harmonic Generation: Driving Inner-Valence Electrons Using Below-Threshold-Energy Extreme-Ultraviolet Light, Phys. Rev. Lett. **117**, 093201 (2016).

[12] K. Kondo, Y. Kobayashi, A. Sagisaka, Y. Nabekawa, and S. Watanabe, Tunneling ionization and harmonic generation in two-color fields, J. Opt. Soc. Am. B **13**, 424 (1996).

[13] T. T. Liu, T. Kanai, T. Sekikawa, and S. Watanabe, Significant enhancement of high-order harmonics below 10 nm in a two-color laser field, Phys. Rev. A **73**, 063823 (2006).

[14] Z. Zeng, Y. Cheng, X. Song, R. Li, and Z. Xu, Generation of an Extreme Ultraviolet Supercontinuum in a Two-Color Laser Field, Phys. Rev. Lett. **98**, 203901 (2007).

[15] W. Hong, P. Lu, P. Lan, Z. Yang, Y. Li, and Q. Liao, Broadband xuv supercontinuum generation via controlling quantum paths by a low-frequency field, Phys. Rev. A **77**, 033410 (2008).

[16] E. Mansten, J. M. Dahlström, P. Johnsson, M. Swoboda, A. L'Huillier, and J. Mauritsson, Spectral shaping of attosecond pulses using two-colour laser fields, New J. Phys. **10**, 083041 (2008).

[17] N. Ishii, A. Kosuge, T. Hayashi, T. Kanai, J. Itatani, S. Adachi, and S. Watanabe, Quantum path selection in high-harmonic generation by a phase-locked two-color field, Opt. Express **16**, 20876 (2008).

[18] L. R. Moore, M. A. Lysaght, L. A. A. Nikolopoulos, J. S. Parker, H. W. van der Hart, and K. T. Taylor, The RMT method for many-electron atomic systems in intense short-pulse laser light, J. Mod. Opt. **58**, 1132 (2011).

[19] T. Ding *et al.*, Time-resolved four-wave-mixing spectroscopy for inner-valence transitions, Opt. Lett. **41**, 709 (2016).

[20] O. Hassouneh, S. Law, S. F. C. Shearer, A. C. Brown, and H. W. van der Hart, Electron rescattering in strong-field photodetachment of F^-, Phys. Rev. A **91**, 031404 (2015).

[21] H. W. van der Hart and R. Morgan, Population trapping in bound states during IR-assisted ultrafast photoionization of Ne^+, Phys. Rev. A **90**, 013424 (2014).

[22] O. Hassouneh, A. C. Brown, and H. W. van der Hart, Harmonic generation by noble-gas atoms in the near-IR regime using ab initio time-dependent *R*-matrix theory, Phys. Rev. A **90**, 043418 (2014).

[23] A. C. Brown, S. Hutchinson, M. A. Lysaght, and H. W. van der Hart, Interference between Competing Pathways in Atomic Harmonic Generation, Phys. Rev. Lett. **108**, 063006 (2012).

[24] O. Hassouneh, A. C. Brown, and H. W. van der Hart, Multichannel interference in high-order-harmonic generation from Ne^+ driven by an ultrashort intense laser pulse, Phys. Rev. A **89**, 033409 (2014).

[25] A. C. Brown and H. W. van der Hart, Influence of multiple ionization thresholds on harmonic generation from Ar^+, Phys. Rev. A **86**, 063416 (2012).

[26] A. C. Brown and H. W. van der Hart, Enhanced harmonic generation from Ar^+ aligned with $M = 1$, Phys. Rev. A **88**, 033419 (2013).

[27] S. Hutchinson, M. A. Lysaght, and H. W. van der Hart, Choice of dipole operator gauge in time-dependent R-matrix theory, J. Phys. B **43**, 095603 (2010).

[28] A. C. Brown, D. J. Robinson, and H. W. van der Hart, Atomic harmonic generation in time-dependent R-matrix theory, Phys. Rev. A **86**, 053420 (2012).

[29] M. D. Perry and J. K. Crane, High-order harmonic emission from mixed fields, Phys. Rev. A **48**, R4051 (1993).

[30] B. Wang, X. Li, and P. Fu, The effects of a static electric field on high-order harmonic generation, J. Phys. B **31**, 1961 (1998).

[31] A. Wirth *et al.*, Synthesized Light Transients, Science **334**, 195 (2011).

[32] A. C. Brown, Two-colour harmonic generation in neon (2016), http://pure.qub.ac.uk/portal/en/datasets/search.html.